Supporting information

Tuning Electronic Structure of Molybdenum Oxide Nanoclusters with Vanadium Doping for Electrochemical H_2O_2 Production

Luyao Zhang,[a,c] Yingbo Li,[a,c] Shuhao Zhang,[b] Jianghua Wu,[a] Weiyang Xue,[a] Kun Wang,[a] Haojie Liu,[a] Boyuan Yu,[a] Xin Zhao,[a] Jiangfeng Ni,[b,*] Feng Yang[a,*]

[a] Department of Chemistry, Southern University of Science and Technology, Shenzhen, 518055, China
[b] School of Physical Science and Technology, Center for Energy Conversion Materials & Physics (CECMP), Jiangsu Key Laboratory of Thin Films, Soochow University, Suzhou 215006, China
[c] These authors contributed equally.
[*]Corresponding authors: E-mail: yangf3@sustech.edu.cn (F. Yang); jeffni@suda.edu.cn (J. Ni)

Chemicals

All chemicals and reagents were obtained from commercial sources and used as received without further purification. Multi-walled carbon nanotubes (CNTs, 10−20 nm in diameter and 0.5−2 μm in length) were purchased from XFNANO, phosphomolybdic acid hydrate ($H_3PMo_{12}O_{40}\cdot nH_2O$), sodium phosphate dibasic heptahydrate ($Na_2HPO_4\cdot 7H_2O$), calcium chloride anhydrous ($CaCl_2$), sodium metavanadate ($NaVO_3$), sodium molybdate (Na_2MoO_4), dimethylformamide (DMF), nitric acid (HNO_3, 68 wt.%) and potassium hydroxide (KOH, AR, 90%) were purchased from Aladdin. sulfuric acid (H_2SO_4, 98%) was purchased from Dong Jiang Regent. Nafion solution (5 wt.%) was purchased from Alfa Aesar China. Cerium sulfate solution (CeS_2O_8, 0.1 N) and ether ($C_4H_{10}O$) were purchased from Macklin.

Supporting Results

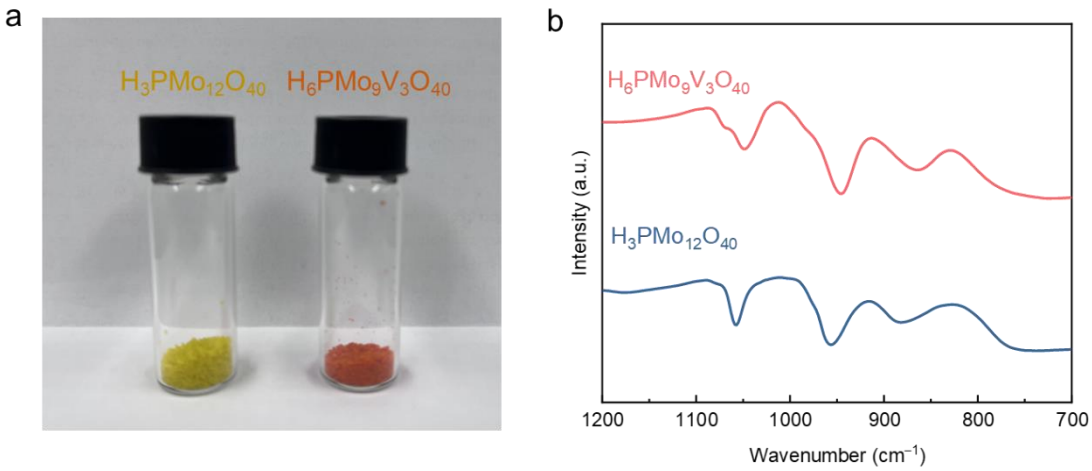

Figure S1. (a) Optical photograph, (b) FTIR spectrum of $H_3PMo_{12}O_{40}$ and $H_6PMo_9V_3O_{40}$.

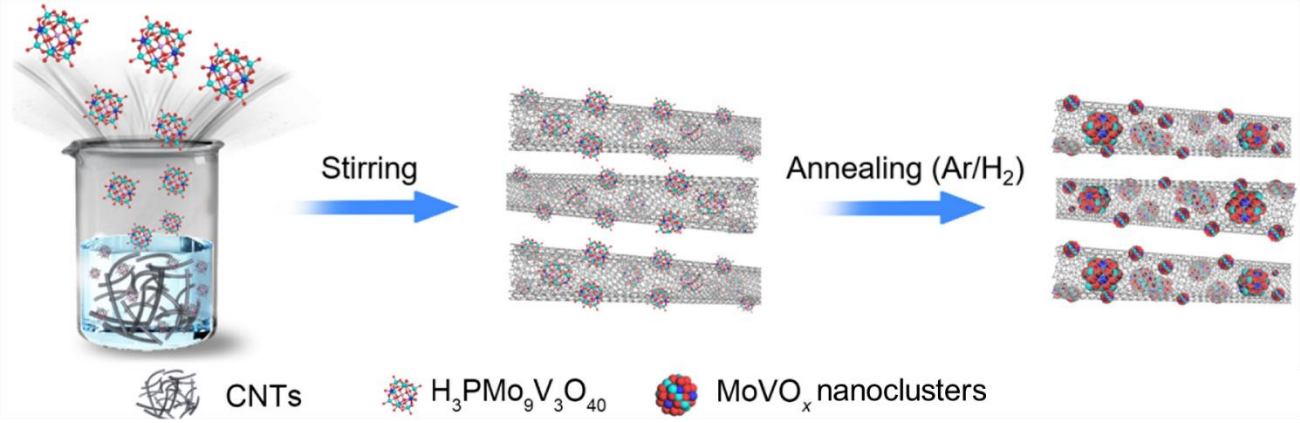

Figure S2. Preparation of the $MoVO_x$ NCs/CNTs catalyst.

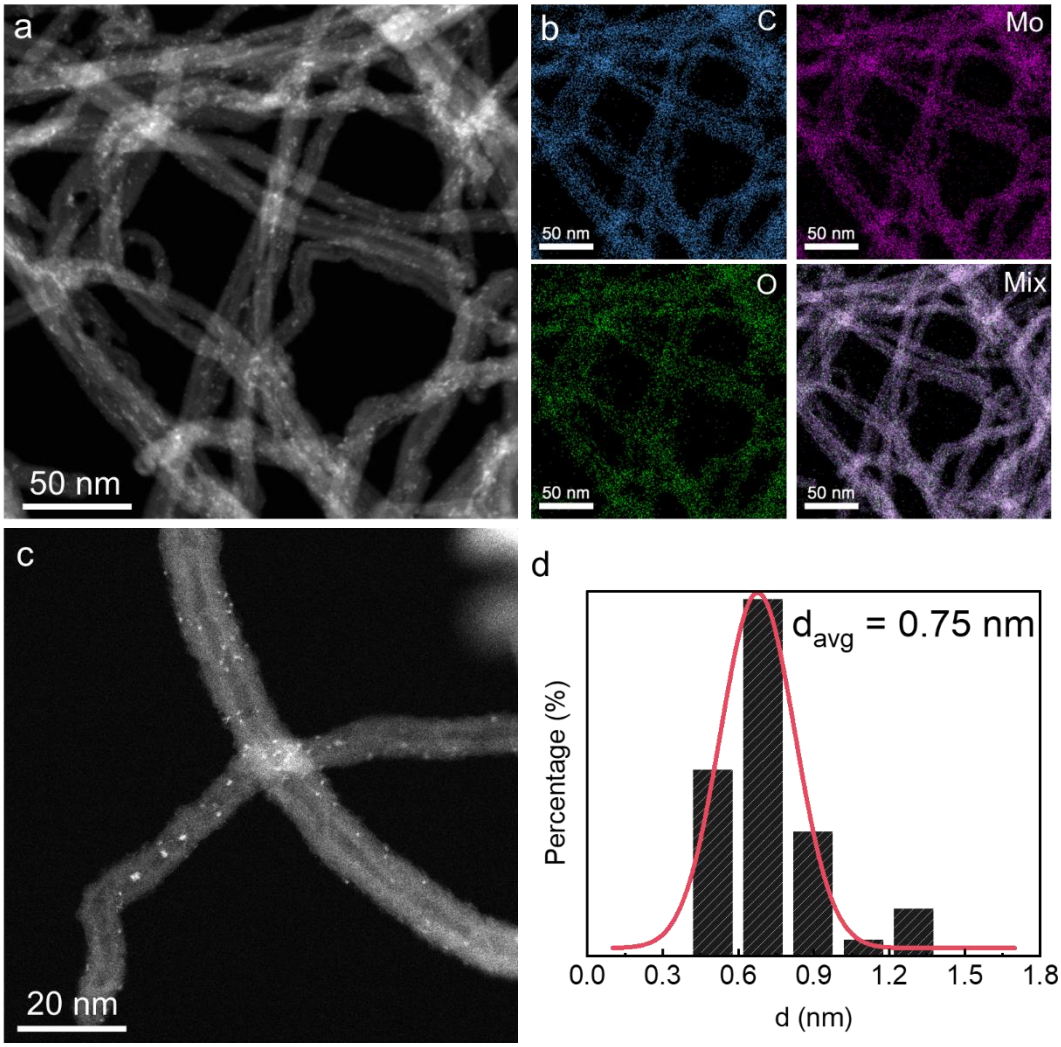

Figure S3. Characterization of MoO_x NCs/CNTs. (a–c) HAADF-STEM image and corresponding STEM-EDX elemental mappings of MoO_x NCs/CNTs. (d) The corresponding particle size distribution of MoO_x NCs within/on CNTs.

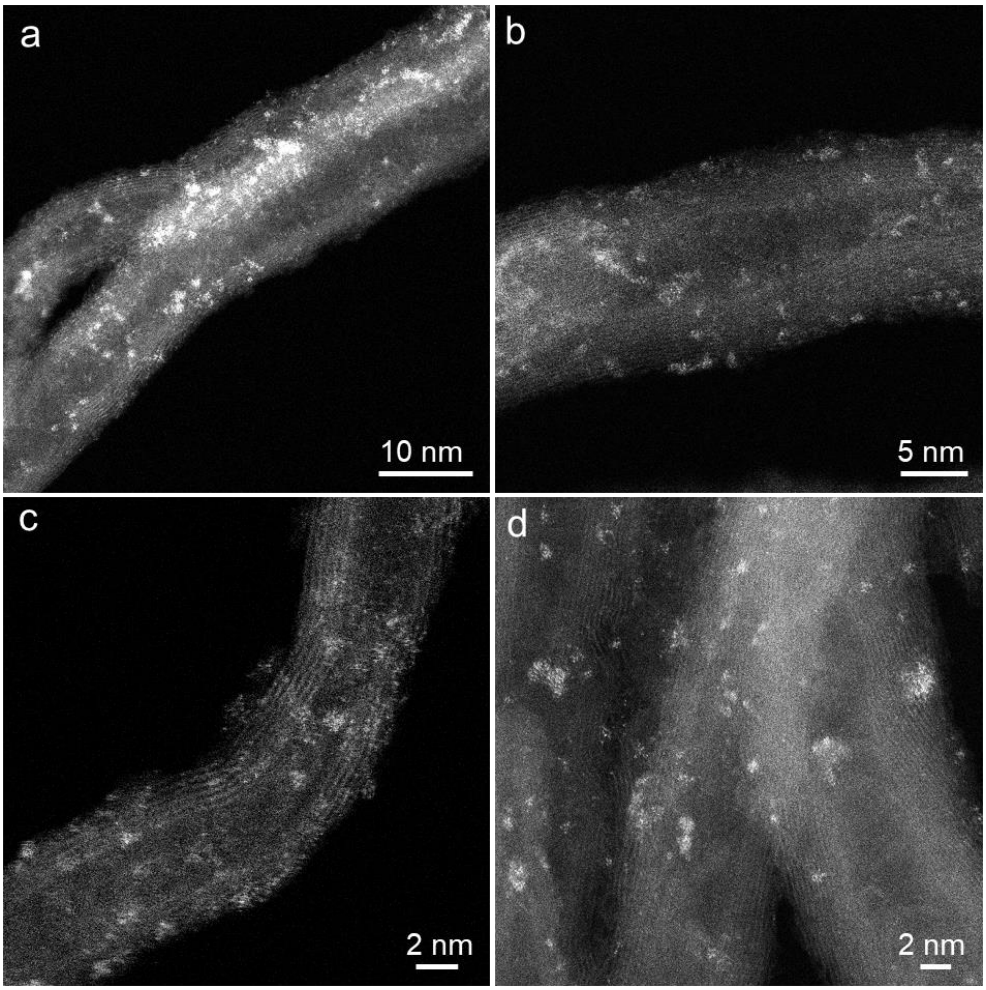

Figure S4. Additional high-resolution HAADF-STEM images of $MoVO_x$ NCs/CNTs.

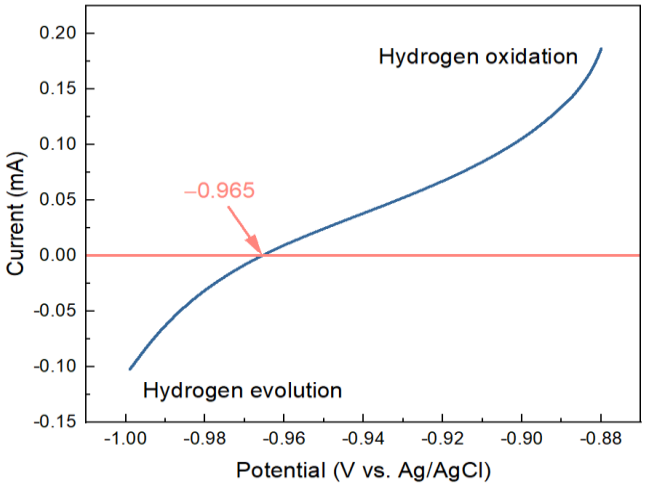

Figure S5. Calibration of the Ag/AgCl reference electrode in H_2-saturated 0.1 M KOH with a sweeping rate of 1 mV/s.

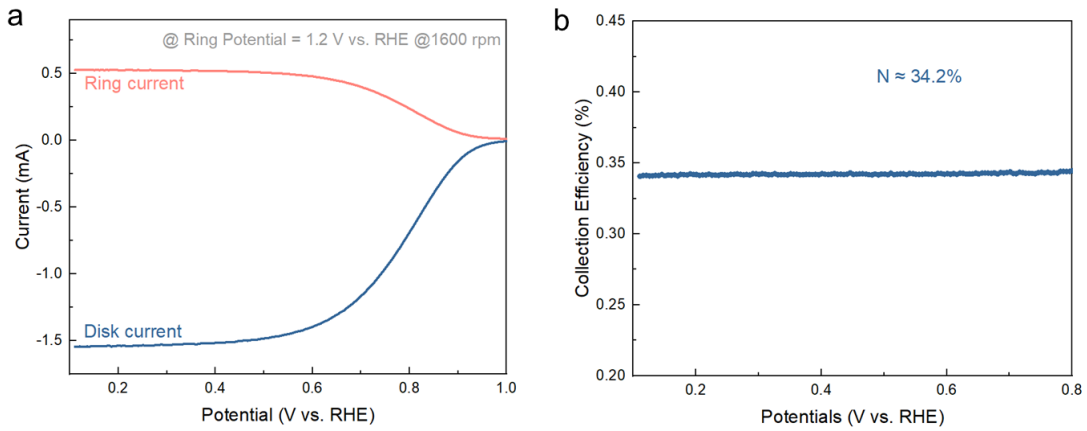

Figure S6. Calibration of the collection efficiency of the bare RRDE in air-saturated 0.5 M KCl with 10 mM $K_3[Fe(CN)_6]$. (a) LSV curve obtained at 1600 rpm with keeping the ring potential at 1.2 V (vs. RHE). (b) The corresponding collection efficiency of RRDE.

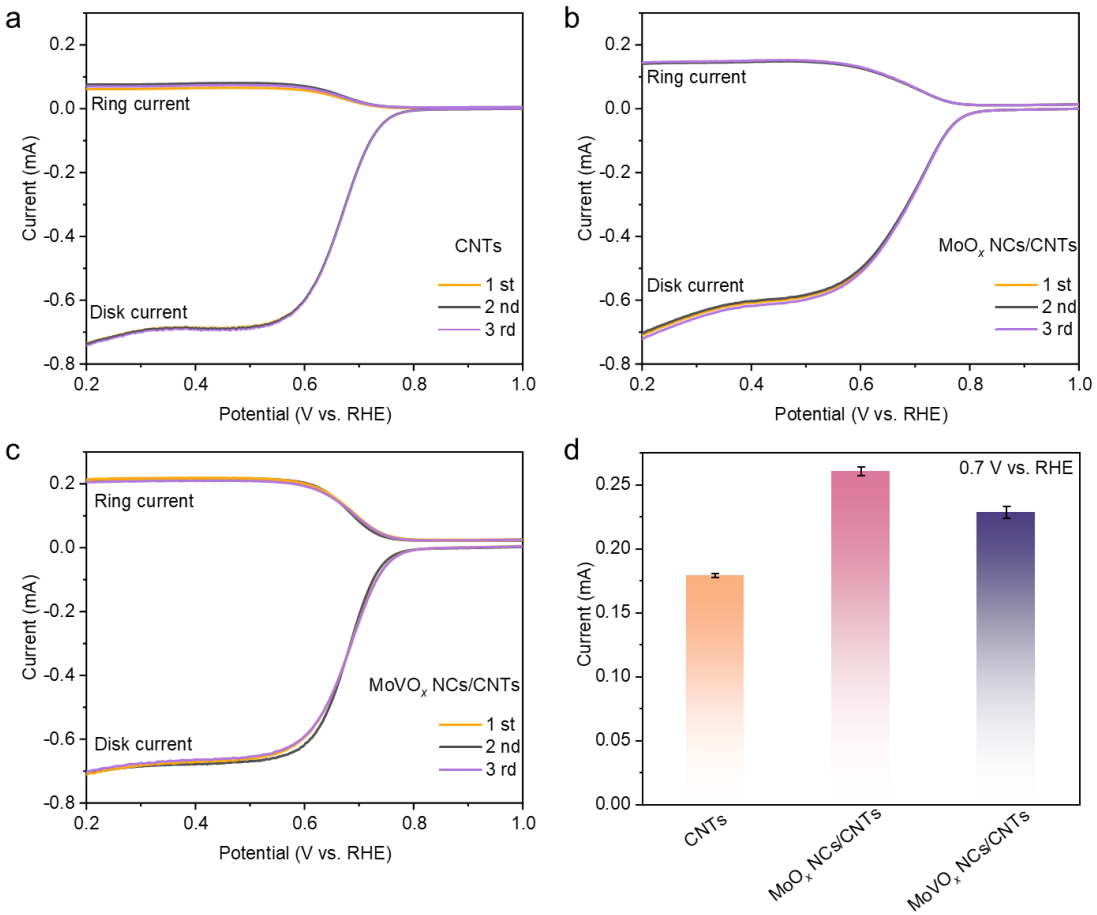

Figure S7. Reproducibility of the ORR performance for the catalysts. (a–c) Disk and ring current of CNTs (a), MoO_x NCs/CNTs (b), and $MoVO_x$ NCs/CNTs (c) measured using three independently prepared samples under identical testing conditions. (d) Reproducibility summary of current calculated at 0.7 V vs. RHE for three catalysts.

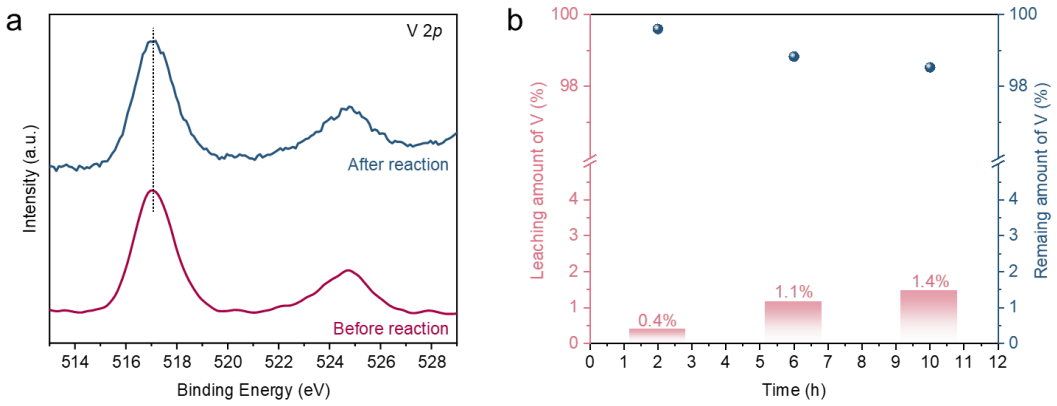

Figure S8. Stability of catalyst. (a) XPS V 2*p* spectra of $MoVO_x$ NCs/CNTs before and after electrochemical measurement. (b) The leaching (left) and remaining (right) of V from $MoVO_x$ NCs/CNTs as a percentage of the original V mass loading during the stability test monitored by ICP-MS.

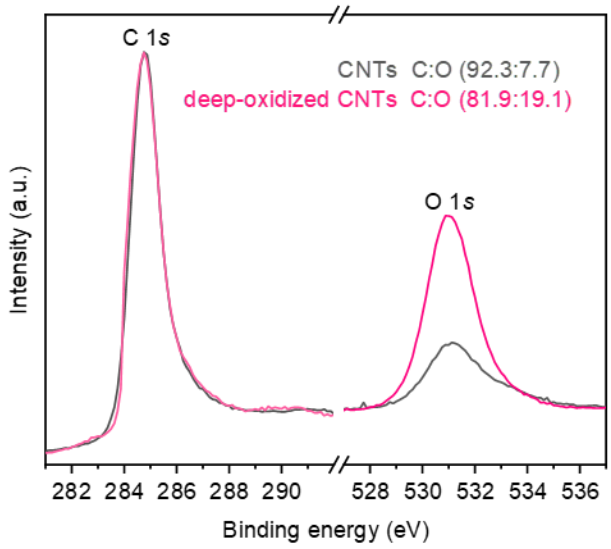

Figure S9. Normalized XPS C 1*s* and O 1*s* spectra of blank carboxylated CNTs and deep-oxidized CNTs. The spectra were normalized with respect to the C 1*s* binding energy peak after energy calibration using SiO_2 reference.

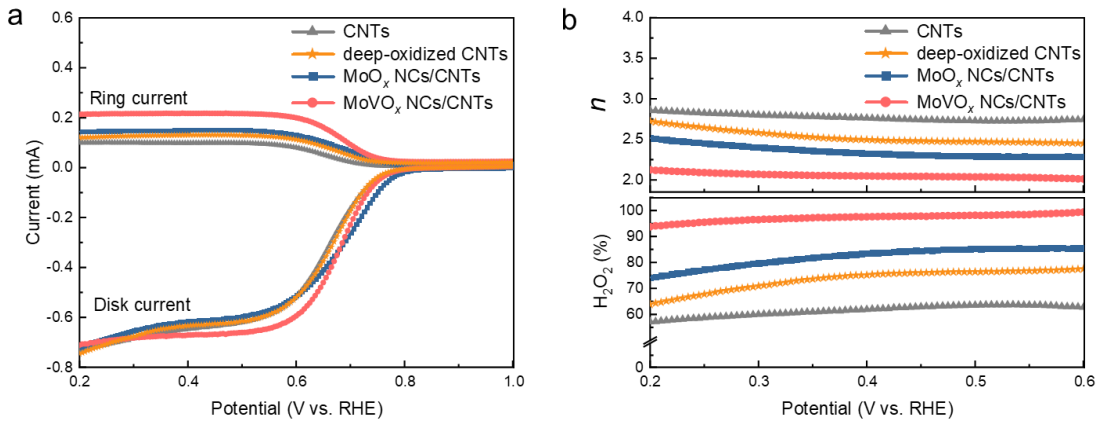

Figure S10. (a) Linear sweep voltammetry (LSV) curves of CNTs, deep-oxidized CNTs, MoO_x NCs/CNTs and $MoVO_x$ NCs/CNTs catalysts. (b) Calculated H_2O_2 selectivity and electron transfer number during the potential sweep.

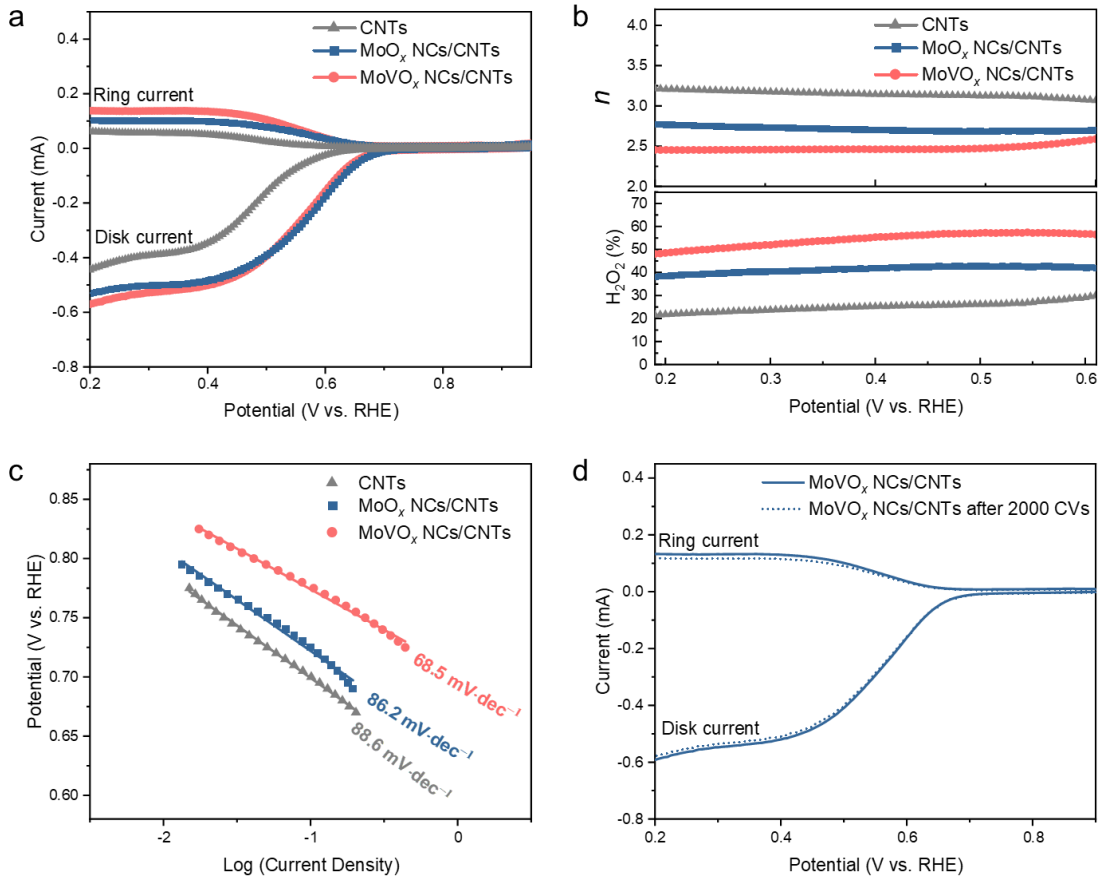

Figure S11. $2e^-$ ORR performance of CNTs, MoO_x NCs/CNTs and $MoVO_x$ NCs/CNTs in 0.05 M H_2SO_4. (a) Disk and ring current of the three samples on the RRDE. (b) The corresponding electron transfer number n and H_2O_2 selection at various potentials. (c) The corresponding Tafel plots. (d) ORR LSV curves of $MoVO_x$ NCs/CNTs before and after 2000 ADT cycles.

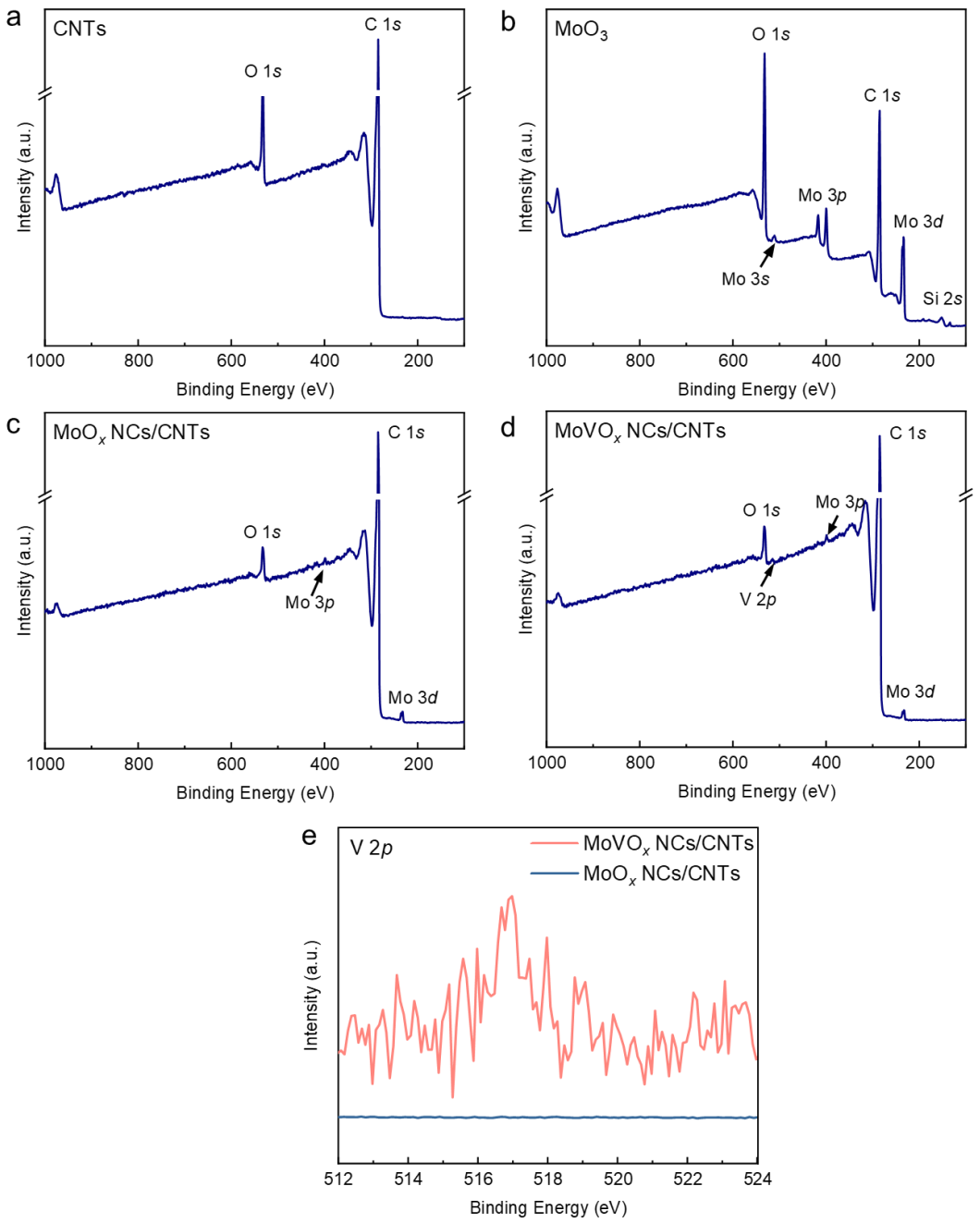

Figure S12. XPS survey spectra of CNTs (a), MoO_3 (b), MoO_x NCs/CNTs (c), and $MoVO_x$ NCs/CNTs (d). (e) High-resolution V 2*p* XPS spectra of MoO_x NCs/CNTs and $MoVO_x$ NCs/CNTs.

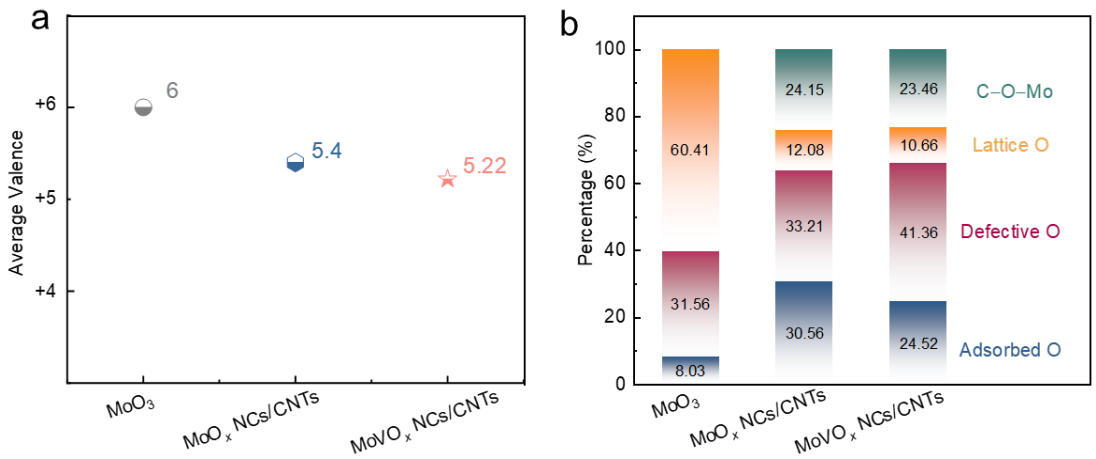

Figure S13. (a) The average valence of MoO_3, MoO_x NCs/CNTs and $MoVO_x$ NCs/CNTs obtained from Mo 3*d* XPS. (b) The distribution of oxygen element in different coordination for MoO_3, MoO_x NCs/CNTs and $MoVO_x$ NCs/CNTs obtained from O 1*s* XPS.

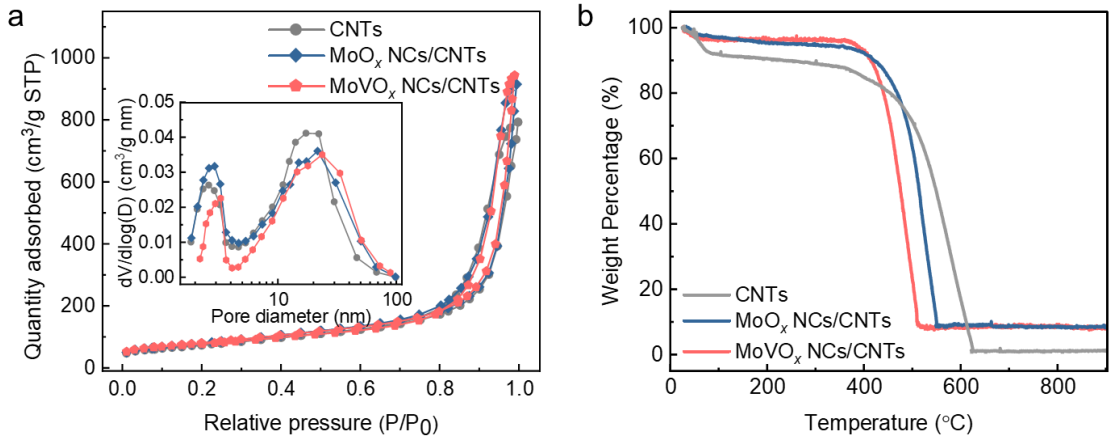

Figure S14. (a) N_2 adsorption/desorption isotherm curves and the pore size distribution profiles (insert), (b) TGA curves of three catalysts.

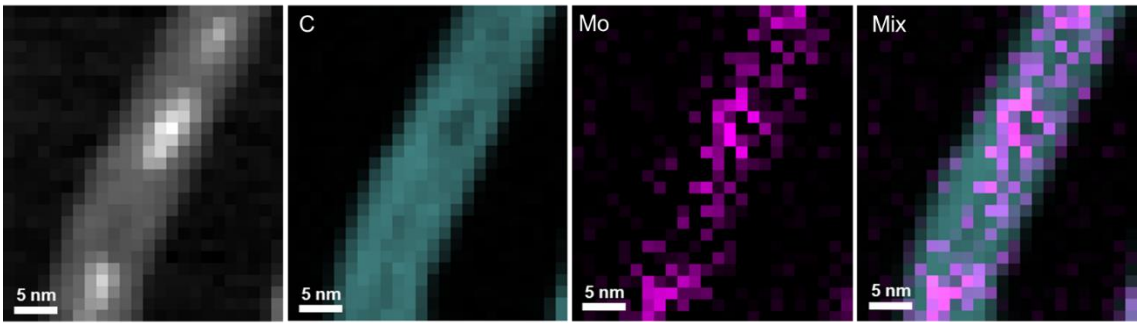

Figure S15. STEM-EELS and corresponding elemental mappings of MoO_x NCs/CNTs.

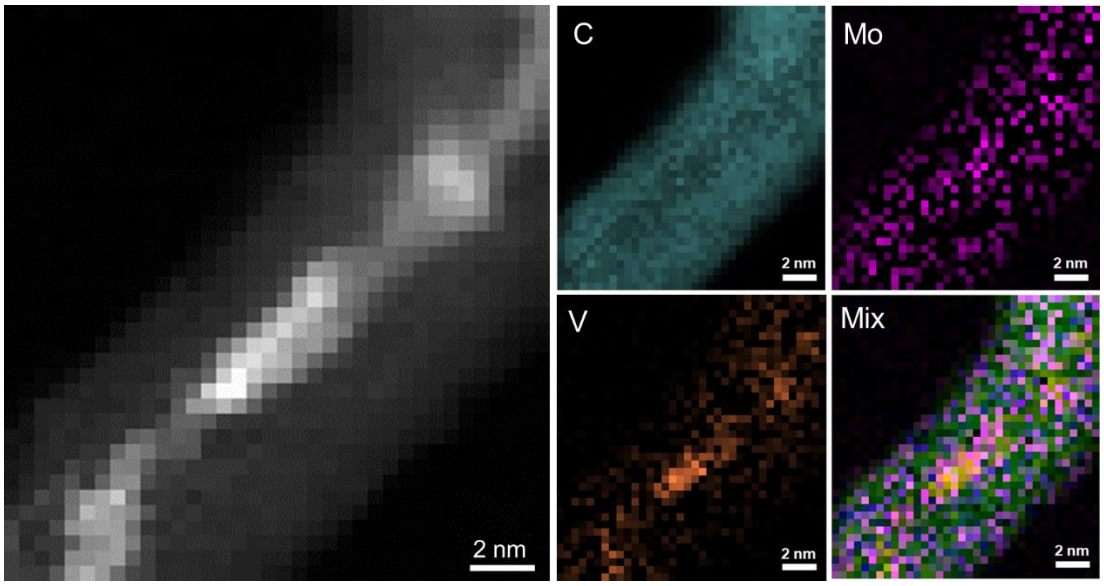

Figure S16. STEM-EELS and corresponding elemental mappings of $MoVO_x$ NCs/CNTs.

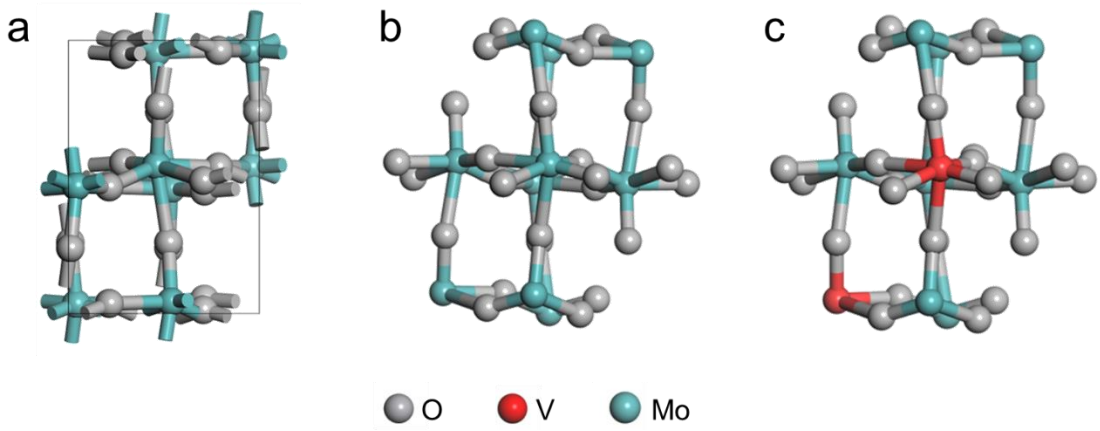

Figure S17. The structural model of MoO_3 (a), MoO_x (b), and V-doped $MoVO_x$ (c).

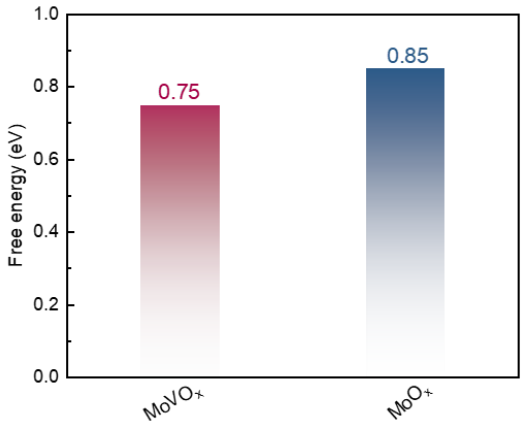

Figure S18. Gibbs free energy of *OOH intermediates on MoO_x and $MoVO_x$ cluster model surfaces.

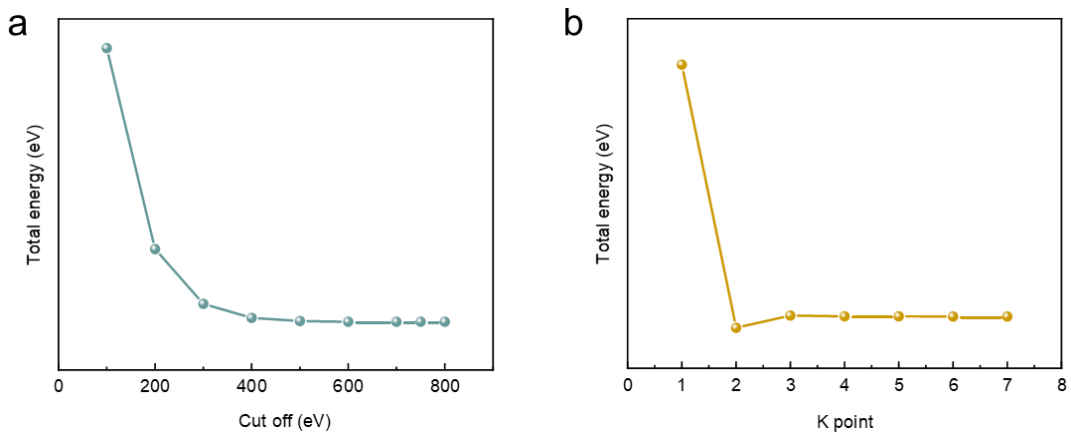

Figure S19. Convergence testing of MoO_3 crystal structure.

Table S1. Performance comparison of electrochemical H_2O_2 production in alkaline media.

Sample	Potential at 1 mA cm^{-2} (V vs. RHE)	H_2O_2 selectivity at 0.4 V	Ref.
$MoVO_x$ NCs/CNTs	**0.7**	**98%**	**This work**
HCNFs	0.72	95%	1
O-CNTs	0.7	90%	2
B/N-HCNS@V_O-G	0.79	91%	3
Oxo-G/NH_3·H_2O	0.68	83	4
o-GOMC-1	0.73	90%	5
BN-C1	0.68	90%	6
MOF-NSs-300	0.66	96%	7
Co-POC-O	0.78	84%	8
Ni_3B	0.7	90%	9
Fe-CNT	0.76	95%	10
Co-N-C	0.8	67%	11
Co1-NGO	0.745	80%	12
g-N-CNHs	0.63	65%	13
Meso C	0.72	77%	14
NCMK3IL	0.68	86%	15
PEI50CMK3_800T	0.72	83%	15
F-mrGO (600)	0.68	100%	16

References

1. K. Dong, J. Liang, Y. Wang, Z. Xu, Q. Liu, Y. Luo, T. Li, L. Li, X. Shi and A. M. Asiri, *Anew. Chem. Int. Ed.*, 2021, **60**, 10583-10587.
2. Z. Lu, G. Chen, S. Siahrostami, Z. Chen, K. Liu, J. Xie, L. Liao, T. Wu, D. Lin, Y. Liu, T. F. Jaramillo, J. K. Nørskov and Y. Cui, *Nat. Catal.*, 2018, **1**, 156-162.
3. Y. Wu, Z. Gao, Y. Feng, Q. Cui, C. Du, C. Yu, L. Liang, W. Zhao, J. Feng, J. Sun, R. Yang and J. Sun, *Appl. Catal., B*, 2021, **298**.
4. L. Han, Y. Sun, S. Li, C. Cheng, C. E. Halbig, P. Feicht, J. L. Hübner, P. Strasser and S. Eigler,*ACS Catal.*, 2019, **9**, 1283-1288.
5. Y. J. Sa, J. H. Kim and S. H. Joo, *Anew. Chem. Int. Ed.*, 2019, **58**, 1100-1105.
6. S. Chen, Z. Chen, S. Siahrostami, D. Higgins, D. Nordlund, D. Sokaras, T. R. Kim, Y. Liu, X. Yan, E. Nilsson, R. Sinclair, J. K. Nørskov, T. F. Jaramillo and Z. Bao, *J. Am. Chem. Soc.*, 2018, **140**, 7851-7859.
7. M. Wang, N. Zhang, Y. Feng, Z. Hu, Q. Shao and X. Huang, *Anew. Chem. Int. Ed.*, 2020, **59**, 14373-14377.
8. B. Q. Li, C. X. Zhao, J. N. Liu and Q. Zhang, *Adv. Mater.*, 2019, **31**, 1808173.
9. F. Ma, S. Wang, X. Liang, C. Wang, F. Tong, Z. Wang, P. Wang, Y. Liu, Y. Dai, Z. Zheng and B. Huang, *Appl. Catal., B*, 2020, **279**, 119371.
10. K. Jiang, S. Back, A. J. Akey, C. Xia, Y. Hu, W. Liang, D. Schaak, E. Stavitski, J. K. Nørskov, S. Siahrostami and H. Wang, *Nat. Commun.*, 2019, **10**, 3997.
11. Q. Zhao, Y. Wang, W.-H. Lai, F. Xiao, Y. Lyu, C. Liao and M. Shao, *Energy Environ. Sci.*, 2021, **14**, 5444-5456.
12. E. Jung, H. Shin, B. H. Lee, V. Efremov, S. Lee, H. S. Lee, J. Kim, W. Hooch Antink, S. Park, K. S. Lee, S. P. Cho, J. S. Yoo, Y. E. Sung and T. Hyeon, *Nat. Mater.*, 2020, **19**, 436-442.
13. D. Iglesias, A. Giuliani, M. Melchionna, S. Marchesan, A. Criado, L. Nasi, M. Bevilacqua, C. Tavagnacco, F. Vizza, M. Prato and P. Fornasiero, *Chem*, 2018, **4**, 106-123.
14. S. Chen, Z. Chen, S. Siahrostami, T. R. Kim, D. Nordlund, D. Sokaras, S. Nowak, J. W. To, D. Higgins and R. Sinclair, *ACS Sustain. Chem. Eng.*, 2018, **6**, 311-317.
15. Y. Sun, I. Sinev, W. Ju, A. Bergmann, S. Dresp, S. Kühl, C. Spöri, H. Schmies, H. Wang, D. Bernsmeier, B. Paul, R. Schmack, R. Kraehnert, B. Roldan Cuenya and P. Strasser, *ACS Catal.*, 2018, **8**, 2844-2856.
16. H. W. Kim, M. B. Ross, N. Kornienko, L. Zhang, J. Guo, P. Yang and B. D. McCloskey, *Nat. Catal.*, 2018, **1**, 282-290.